Polymacromonomers: Structure and Dynamics in Nondilute Solutions, Melts, and Mixtures

D. Vlassopoulos,*,† G. Fytas,† B. Loppinet,† F. Isel,‡ P. Lutz,‡ and H. Benoit‡

Foundation for Research and Technology-Hellas (FO.R.T.H.), Institute of Electronic Structure & Laser, P.O. Box 1527, 71110 Heraklion, Crete, Greece, and Institut Charles Sadron (CNRS-ULP), 6, rue Boussingault, 67083 Strasbourg Cedex, France

Received April 11, 2000; Revised Manuscript Received May 22, 2000

ABSTRACT: Polymacromonomers are viewed as a special class of well-characterized branched polymers with high density of arms and shape ranging from spherical to nonspherical, depending on the arm functionality and molecular mass. We synthesized a series of such model systems with polystyrene or poly(methyl methacrylate) backbone and varying functionality and/or molecular mass of polystyrene arms and investigated their structure and dynamics in nondilute solutions (well above the overlapping concentration c^*) and in the melt. We found similarities in their soft ordering and dynamic response with other well-known model branched polymers such as multiarm stars, in that cooperative and self-diffusion or arm relaxation and structural rearrangements control their dynamics in solution or in the melt, respectively. However, the present systems do not follow the scaling laws of stars as a consequence of their anisotropy and the larger interpenetration needed to observe the effect of ordering on the dynamic response. The use of blends consisting of different polymacromonomers essentially enhances the polydispersity, enabling the detection of the self-diffusion mode in analogy to the multiarm stars, as well as obtaining a wide range of effective intermediate molecular masses, depending on composition. The mixtures investigated were miscible at all times and exhibited a dynamics dominated by the response of the slower components. These polymers complement the generic physical picture of the dynamics of branched polymers toward the low arm molecular mass.

I. Introduction

Branched polymers in the form of star-shaped polymers or polymacromonomers exemplifying spherical or cylindrical polymer brushes, respectively, represent special cases of tethered chain systems[1] and can be synthesized via various synthetic routes. Star-shaped polymers are characterized as species where all the chains (arms) of one molecule are connected to a central point, the core. The most efficient method to obtain well-defined star-shaped polymers with controlled arm length and functionality is the use of chlorosilane chemistry yielding dendritic cores of different generations and numbers of arms as high as $f = 128$.[2] The subsequent anionic polymerization leads to nearly monodisperse spherical core/shell structures with soft colloidal character evident from the formation of liquidlike ordering.[3−5] The static and dynamic properties of the third ($f = 64$) and fourth ($f = 128$) generation of polybutadiene stars have been the subject of recent experimental and theoretical work in nondilute solutions[2,3] and melts.[5] These systems exhibit rich dynamics reflecting their weak spatial core−core correlation. The appropriate use of various spatial and temporal experimental techniques allows distinguishing the various relaxation mechanisms relating to arm and core (structural) modes of motion. Over the years several other synthetic methods have been developed. They have been discussed in detail elsewhere.[6]

Polymacromonomers (abbreviated as PM's) are also highly branched species where each monomer unit of the backbone incorporates a grafted macromonomer. Their homopolymerization basically refers to anionic[7] or mostly to free radical[8] polymerization processes, yielding spherical or nonspherical overall shapes, depending upon the length of the backbone, and allowing for chemically different backbone and grafts. Recently, atom transfer radical polymerization was proven to be a particularly effective means of synthesizing PM's.[9] These materials have been mostly studied in dilute solution so far,[10] with emphasis on their molecular shape and dimensions, which were investigated using primarily light scattering and viscosimetry. There is also work carried out in the bulk state and in particular in issues relating to the glass transition and film-forming properties, as well as the presence of liquid crystalline mesophases resulting from the molecular anisotropy;[11,12] the latter behavior was also observed in solutions at high volume fraction. One important outcome from these studies relates to the change of molecular shape from nearly spherical starlike to rodlike as the number and length of grafted arms increase. In some cases bottle−brush structure could be evidenced.[13,14] Significant progress has been reported in the simulation and modeling of PM's and in particular the effects of the backbone and graft (arm) sizes on their shape and dimensions,[14,15] which confirm the experimental findings.[10−13] An interesting aspect is the analogy of PM's with comb polymers having high arm density, with respect to their anisotropic shape and the relative importance of backbone and arm sizes.[15,16] However, neither a systematic investigation of the influence of the structure in dilute solutions has been made, nor a comparison to hyperstars to examine whether a similar description of the form factor $P(q)$ is possible.

To define the unifying principles that control the dynamic behavior of branched polymers such as multiarm stars, combs, and PM's (typically with chemically dissimilar backbone and grafts), as well as the strength of

† Foundation for Research and Technology-Hellas.
‡ Institut Charles Sadron.

10.1021/ma000634q CCC: $19.00
Published on Web 07/12/2000

Table 1. Molecular Characterization of the Polymacromonomers (PM) Utilized

sample	back-bone	$M_{w,branch}$[a]	$M_{w,PM}$[b]	f[c]	c^* (wt %)[d]	R_h[e] (nm)
PMM10-g-S20	PMMA	2100	23 500	10	6.5	3
PMM40-g-S20	PMMA	2100	82 100	40	5	4[f]
PMM10-g-S110	PMMA	11 800	103 600	10	4	6
PMS10-g-S100	PS	10 000	99 600	10	4	6

[a] $M_{w,branch}$: weight-average molar mass (in g/mol) of the macromonomer precursor, i.e., the actual graft in the polymacromonomer, determined by size exclusion chromatography (SEC), measured in g/mol. The polydispersity indices are about 1.05. [b] $M_{w,PM}$: weight-average molar mass of the polymacromonomer determined by light scattering (LS) in THF or SEC on line with LS. The polymacromonomers were free of precursor, and the polydispersity indices were estimated as 1.1. [c] f: average polymerization degree resulting from the ratio $M_{w,PM}/M_{w,branch}$, which is effectively the functionality of the PM. [d] Obtained from dynamic LS measurements (see text and Figure 2). [e] Hydrodynamic radius obtained from dilute solution dynamic light scattering measurements (see text). [f] See also text for consideration of anisotropy.

their colloidal vs polymeric character, one should utilize a wide range of well-defined polymeric systems with varying molecular parameters and macromolecular shapes varying from spherical to nonspherical. In this respect, the use of model high arm density comblike polymers, and in particular polymacromonomers, is necessary as it complements and extends the previous work on (regular) spherical star polymers to other classes of branched polymers with shape−structure−dynamics interplay.

In this work, we have selectively synthesized four polystyrene (PS) and poly(methyl methacrylate) (PMMA) based macromonomers of controlled structure, yielding spherical and nonspherical shape, average number of branches $f = 10$ and 40 and two different arm lengths ($N_a = 20$ and 100). Their structure−dynamics interplay was monitored with dynamic light scattering, shear rheology, and small-angle X-ray scattering (SAXS). The enhanced osmotic pressure, the cooperative diffusion, and the contributions of the composition fluctuations (seen as "core" density fluctuations) of semidilute and concentrated solutions in the good solvent toluene were resolved and compared with corresponding theoretical results and predictions of interacting multiarm star polymers with inherent segment density heterogeneity.[4] Significant arm (graft) interpenetration beyond that of hyperstars is evidenced from the dynamic properties above the overlapping concentration c^*. Further, the effect of the topological asymmetry was examined by using mixtures of two different PM's, whereas the influence of PM functionality and arm molecular mass on the dynamic behavior in the melt state was also investigated. All blends used here were thermodynamically compatible.

At this point a note concerning the comparison of the present polymacromonomers with regular multiram stars, which is discussed throughout this work, is in order. Such a comparison is justified on two grounds: (a) the need to explore the validity of the scaling laws derived for the regular stars,[4] to other branched polymers, more complicated, which however exhibit some common features with the stars, and (b) the fact that, with only one exception, the polymacromonomers used in this work seem to have a conformation that does not deviate sharply from that of regular spherical stars. This is due to their low functionality and low arm molecular weight, as discussed in detail in the following sections and summarized in Table 1. These molecular characteristics suggest a clear resemblance of the present polymacromonomers with those investigated in ref 10 and at the same time a sharp contrast from the ones discussed in ref 13; in the latter case, the "bottle−brush" polymers had much higher functionality and total molecular weight (with a range of small arm molecular weights), yielding highly anisotropic objects with typical persistence length of the order of 100 nm. The outcome of this comparison can serve as a guide for identifying what needs being taken into account in order to describe the properties of polymacromonomers of varying degree of nonsphericity.

II. Experimental Section

Materials. The polystyrene macromonomers were prepared by induced ionic deactivation according to a method published earlier in the literature.[7] Briefly, once the polymerization of styrene was completed, the "living" anions were reacted first with a slight excess of oxirane and then with an appropriate unsaturated electrophile, such as methacryloyl chloride, for the poly(methyl methacrylate), PMMA, macromonomers fitted with polymerizable methyl methacrylate end groups or vinylbenzyl bromide (or chloride) and for the polystyrene, PS, macromonomers fitted with end-standing polymerizable styrene units. In the latter case, an intermediate addition of 1,1-diphenylethylene was necessary to avoid side reaction during the deactivation. These different samples were submitted to a detailed characterization to confirm the expected structure. The polymacromonomers were prepared by anionic homopolymerization of the macromonomer. In particular, the sample was freeze-dried in order to remove the remaining protonic impurities; the homopolymerization of the ω-methacryloyloxy PS macromonomers was carried out in THF (free of any impurities) at low temperatures generally in the presence of LiCl, the ratio [LiCl]/[LE] (living ends) being equal to 5. As initiator, 1,1-diphenylmethylpentyllithium-3 (DPMPLi) was used, at an amount depending upon the desired polymerization degree. The macromomer solution was added rapidly to the THF solution containing the initiator. The coloration of the reaction mixture vanished immediately, confirming the consumption of the initiator. The reaction mixture was then kept at constant temperature until complete conversion. At given times, samples were taken out for purpose of characterization by size exclusion chromatography and light scattering. Thus, both the conversion, i.e., the incorporation of the macromonomer, and the molar mass of the branched species could be obtained. In some cases unreacted macromonomer had to be removed from the final sample by fractional precipitation using toluene/methanol. The homopolymerization of the (ω-styryl)polystyrene macromonomer was conducted in benzene solution at room temperature using *sec*-butyllithium as initiator. The main molecular characteristics of the PM's used in this work are presented in Table 1 and discussed in the rest of the paper.

Dilute solutions (or blend solutions) in good solvent toluene were prepared by dissolving the appropriate amount of PM in the solvent (toluene) for about 12 h. Concentrated solutions were obtained by slow evaporation of the original dilute batches under vacuum at room temperature; depending on the desired concentration this procedure could take up to 2 days. Melts (or blends) were obtained through complete removal of toluene under vacuum, over a period of 1 week. All solutions measurements were carried out at 20 °C.

Dynamic Light Scattering (DLS). High-quality intermediate scattering functions $C(q,t) = ((G(q,t) - 1/f^*)^{1/2})$ (f^* is the instrumental coherence factor, obtained by means of a standard) were computed under homodyne conditions from the experimental polarized (VV) light scattering intensity autocorrelation function $G(q,t)$ measured at a wavevector $q = (4\pi n/\lambda) \sin \theta/2$ (λ is the laser wavelength, n the refractive index, and θ is the scattering angle) with an ALV-5000 correlator over a broad time range ($10^{-7}-10^3$ s). The experimental setup

included a Nd:YAG laser operating at 532 nm and an ALV goniometer. The analysis of $C(q,t)$ proceeded via the inverse Laplace transformation (ILT) assuming a superposition of exponentials:

$$C(q,t) = \int_{-\infty}^{\infty} L(\ln \tau) \exp(-t/\tau)\, d \ln \tau \qquad (1)$$

with τ being the characteristic relaxation time of a process. The ILT, which was realized using the program CONTIN,[17] allowed the determination of the relaxation time and intensity of the partitioning modes, as revealed by the distribution relaxation function $L(\ln \tau)$. Further details are discussed elsewhere.[4,18]

Shear Rheology. The viscoelastic properties of the polymacromonomers in solution and in the melt were measured with Rheometric Scientific ARES rheometers. In the former case a high-resolution force rebalance transducer 100 $FRTN_1$-HR was utilized in conjunction with cone and plate geometry (diameter 25 mm, angle 0.04 rad) and circulating fluids bath, whereas in the latter case a standard transducer 2K $FRTN_1$ was used along with 8 mm parallel plates and flowing N_2 temperature control. Dynamic frequency sweeps at different temperatures in the range 90−170 °C were carried out in order to characterize the dynamic response of the test systems. The linear viscoelastic limits were identified with dynamic strain sweep tests. In addition, steady rate sweep experiments were performed in order to measure the shear viscosities, in particular in the lower concentration solutions where the dynamic moduli could not be accurately resolved.

Small-Angle X-ray Scattering (SAXS). Small-angle X-ray scattering experiments were performed at room temperature (20 °C) with a Rigaku small-angle diffractometer (model D/max-2400). Ni-filtered Cu Kα radiation from a 12 kW rotating anode (Rigaku) was used. The beam was collimated by a system consisting of three parallel slits, resulting in a beam size of 0.2 × 30 mm hitting the sample. The scattered intensity was collected on a linear position-sensitive proportional counter (Rigaku) situated 25 cm away from the sample. The intensity was corrected from background scattering and desmeared for slits height using the method of Strobl.[19]

III. Results and Discussion

Dilute Solution Characterization. DLS measurements in dilute solutions with concentrations c below the overlap concentration c^* revealed one relaxation process with an intermediate scattering function $C(q,t) = \alpha \exp(-q^2 D_0 t)$, corresponding to an intensity $I_0 = \alpha I$, where α is the amplitude of $C(q,t)$ at $t > 1$ μs and I is the total polarized light scattering intensity (at a certain q); I_0 arises exclusively from concentration fluctuations. From the translational diffusion (at $c \rightarrow 0$) $D_0 = kT/(6\pi\eta_s R_h)$ (η_s is the solvent viscosity, T the temperature, and k the Boltzmann constant) the hydrodynamic radius R_h of the PM can be readily obtained, under the assumption of spherical symmetry. Among the four PM's studied, the PMM10-g-S110 and PMS10-g-S100 were found to have experimentally the same $R_h = 6$ nm (Table 1), whereas R_h assumed the values 3 and 4 nm for PMM10-g-S20 and PMM40-g-S20, respectively; the rather low value of the latter suggests nonspherical shape. These considerations are based on the previous experience[10−11,13−16] with PM's of systematically varying arm number and length, which imply that in the present test systems the PMM40-g-S20 is the more anisotropic, whereas the others can be reasonably well approximated with spherical objects. Therefore, in the latter case one can argue that the entropy gain from a Gaussian coil attributed to the PS grafted chains is larger than the entropic loss due to backbone exntension.[10,15] In view of the lack of dynamic depolarized intensity necessary to estimate the rotational diffusion within the experimentally accessible time window, we approximated the PMM40-g-S20 with a prolate ellipsoid having semiaxes a and b, based on earlier considerations on the matter already reported in the literature;[10,13,14] in this case the translational diffusion is $D_0 = kTG(\rho)/(6\pi\eta_s a)$ where $G(\rho) = (1 - \rho^2)^{-1/2} \ln[(1 + (1 - \rho^2)^{1/2})/\rho]$ and $\rho \equiv b/a < 1$.[18] The combination $a = 6$ nm and $b = 3$ nm is compatible with the experimental value of D_0 and seems to be more realistic in view of the R_h value of the nearly spherical starlike PMM10-g-S100 with similar total molecular mass.

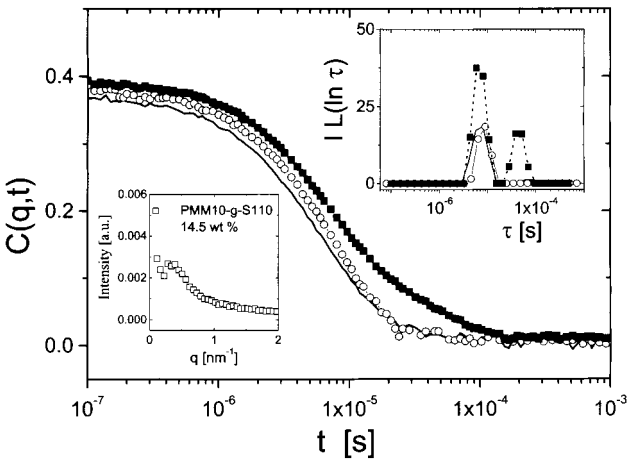

Figure 1. Autocorrelation function of the concentration fluctuations $C(q,t)$ with $q = 0.034$ nm^{-1} for PPM10-g-S20 15.8 wt % (○), PMM40-g-S20 15.2 wt % (solid line), and their mixture (60 wt % in PMM40-g-S20 and 13.8 wt % total polymer concentration; ■) in toluene at 25 °C. Upper inset: the corresponding distribution of relaxation times $L(\ln \tau)$, eq 1, multiplied by the total scattering intensity I for comparison. Lower inset: SAXS intensity profile of PMM10-g-S110 in toluene (14.5 wt %, □), demonstrating liquidlike ordering.

Nondilute Solutions. Cooperative Diffusion. With increasing concentration, $I_0(c)$ assumed its maximum value at c^* as discussed below. Figure 1 shows experimental $C(q,t)$ for PMM40-g-S20 and PMM10-g-S110 respectively at 15.2 wt % (about $3c^*$) and 15 wt % (about $4c^*$), at $q = 0.034$ nm^{-1}(see also Table 1 and Figure 2). The experimental $C(q,t)$ of the latter was well described by a single exponential even at concentrations well into the semidilute regime, in contrast to multiarm stars,[4] which are characterized by a more complex $C(q,t)$, even at concentrations slightly below c^*. On the other hand, the PMM40-g-S20 exhibited a weak slow relaxation process. As already mentioned, to accurately resolve the various modes, we employed an inverse Laplace transformation of $C(q,t)$ to obtain the distribution $L(\ln \tau)$ of relaxation times (eq 1). In fact, $L(\ln \tau)$ (upper inset of Figure 1) revealed the presence of a second weaker and slower diffusive process. The fast process was the expected cooperative diffusion responsible for the relaxation of the total polymer concentration fluctuations, whereas the slow process (in PMM40-g-S20) was probably associated with the PM self-diffusion. Much like the case of multiarm stars, the slow process in the light scattering experiment can arise from functionality or size polydispersity. This assignment is strongly supported by the strong intensity enhancement of this process in the mixture PMM40-g-S20/PMM10-g-S110 shown by the second peak of $L(\ln \tau)$ in Figure 1, in harmony with earlier investigations on mixtures of multiarm star polymers.[20]

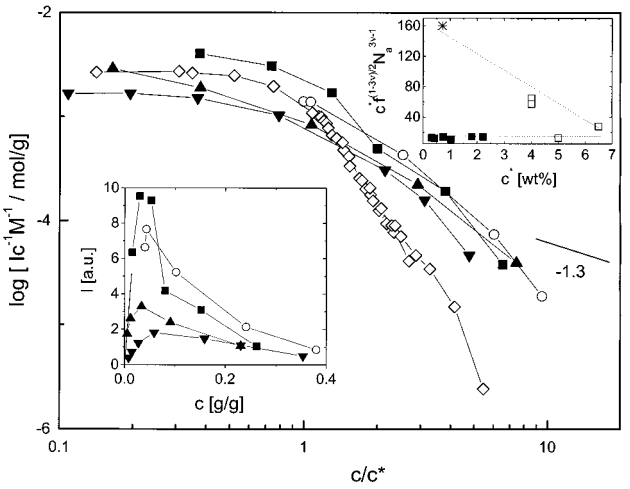

Figure 2. Normalized light scattering intensity per scatterer (I/cM) due to the total concentration fluctuations (cooperative diffusion) versus the reduced concentration c/c^* for all samples investigated: PMM10-g-S20 (▼); PMM40-g-S20 (■); PMM10-g-S110 (▲); PMS10-g-S100 (○). For comparison, respective data from polybutadiene multiarm star PB6407[3] (◇) are also shown. The solid line with slope −1.3 represents the scaling for semidilute linear homopolymers (eq 1). Lower inset: the corresponding concentration dependence of the light scattering intensity (normalized to the intensity of toluene) as a function of concentration (exhibiting a peak at the overlap c^*). Upper inset: representation of the scaling of the overlapping concentration for star polymers $c^* \sim (f^{1/2}N_a)^{3\nu-1}$ (see text); data for stars of functionalities $f = 64$ and 128 (■) demonstrate the validity of this scaling prediction. On the other hand, data for the PM's (□; see also Table 1) as well as a linear PB with M_w = 165 000 g/mol (*) clearly deviate from this prediction. It is interesting that the c^* with the highest functionality PMM40-g-S20 (c^* = 5%) seems to comply with the star scaling. The dotted lines are drawn to guide the eye.

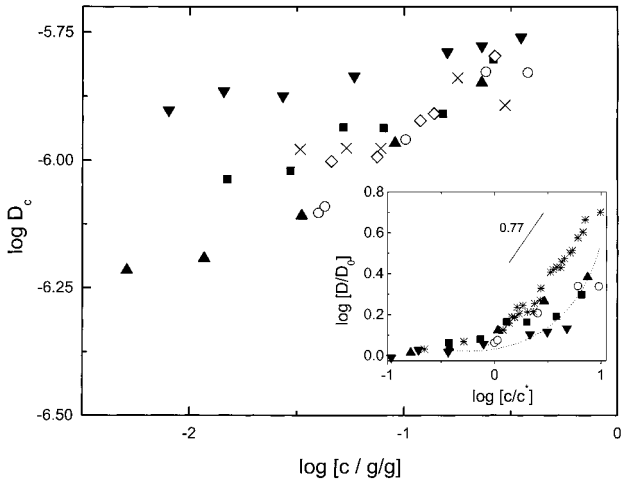

Figure 3. Concentration dependence of the (cooperative) diffusion coefficient for the concentration fluctuations in the four samples (symbols are the same as in Figure 2) and the two mixtures (PMM40-g-S20/PMM10-g-S20, ×; PMM40-g-S20/PMM10-g-S110, ◇). Inset: the reduced cooperative diffusion D_c/D_0 vs reduced concentration c/c^* for the PM's, along with the corresponding data for PB6407 (*). The solid line with slope 0.77 represents the scaling for semidilute linear homopolymers (eq 2), and the dotted curve is drawn to guide the eye.

The lower inset of Figure 1 depicts a typical SAXS intensity profile of PMM10-g-S110 in toluene at a concentration of 14.5 wt %. A soft liquidlike ordering is clearly observed, characterized by a low-q broad peak and very weak secondary broader peaks at higher q's. The excess scattering at the lowest q's is an experimental artifact typically encountered in polymeric systems.[5] From the study of different concentrations, the extracted "interparticle" distance $d = 2\pi/q_{max}$ seems to conform to the scaling $d \sim c^{-1/3}$, in agreement with the soft ordering of multiarm star polymers (and in particular the star 6407 considered in this work, among other stars)[2,21] and block copolymer micelles,[22] suggesting a uniform reduction of the domain spacing in all three dimensions as the concentration is increased.

Figures 2 and 3 summarize the results in terms of the reduced intensity I/cM (c is the concentration and M the total molecular mass) and cooperative diffusion coefficient D_c in the four systems of Table 1. The former is inversely proportional to the osmotic compressibility $(\partial\Pi/\partial c)_{P,T}$ of the solution which expectedly increases with c above c^*.[4,23] This is demonstrated in the $I(c)$ vs c plot of the inset of Figure 2, exhibiting a maximum at c^*. The deduced values of the overlap concentration are listed in Table 1. For multiarm stars (with $f \geq 64$) the overlap concentration conforms to the scaling[4] $c^* \sim (f^{1/2}/N_a)^{3\nu-1} = f^{0.33}N_a^{-0.77}$ where $\nu = 0.59$ is the Flory exponent for good solvent and N_a is the degree of polymerization of the star arm (see Figure 2). However, this scaling in not applicable in the present case as evidenced from the similar c^* values of PMM10-g-S110 and PMM40-g-S20 with different f and N_a (Table 1); the multiarm star scaling would require more than 6 times higher c^* for the latter. The c^* values of the polybutadiene (PB) multiarm stars (f = 64 and 128) and the present PM's are shown in the upper inset of Figure 2, along with the corresponding value of a linear PB (M_w = 165 000 g/mol) for comparison. The different f and N_a dependence of c^* of the polymacromonomers with spherical starlike shape ($f = 10$) can be rationalized by considering R_g (or R_h) as a sum of contributions from the core ($\propto f^{1/2}$) and the corona ($\propto N_a^{1/2}$), i.e., a different functional dependence from that of the hyperstars.[2]

The osmotic modulus $(\partial\Pi/\partial c)_{P,T}^{-1}$ in semidilute solutions can be still plotted against reduced concentration c/c^* (Figure 2). In the established case of (spherical) multiarm stars, the inhomogeneous segment concentration profile from the core to the shell modifies the concentration scaling of the intensity for semidilute linear homopolymers by a factor relating to the shell/core thickness ratio:[4]

$$\frac{I_c}{cM} \propto c^{-0.3}\left[1 + 0.21(1+\delta)\left(\frac{c}{c^*}\right)^{-1.3}\right] \qquad (1)$$

where 0.21 stands for $(3\nu - 1)/(3\nu)^{3\nu/3\nu-1}$ and δ is a measure for the difference in the chain stretching in the nonuniform (core) and homogeneous (shell) regions. Compared to the standard good-solvent scaling[23] $c^{-1.3}$, the correction term in eq 1 gives rise to a stronger decrease of I_c with c. This is also apparent in Figure 2, which depicts the respective cooperative diffusion data of a multiarm star polybutadiene with $f = 64$ arms and arm molecular mass about 7000 g/mol (coded as PB6407),[4] measured in the good solvent cyclohexane. This polymer is the closest regular hyperstar to PM's, and in particular its dimensions ($R_g \cong 10$ nm)[4b] are not far from those of the anisotropic PMM40-g-S20. Therefore, it can be considered as the "spherical analogue" of PMM40-g-S20.

It is noted that in the concentration range above c^* the normalized intensities do not truly collapse into a master curve; this is not an unexpected finding, as

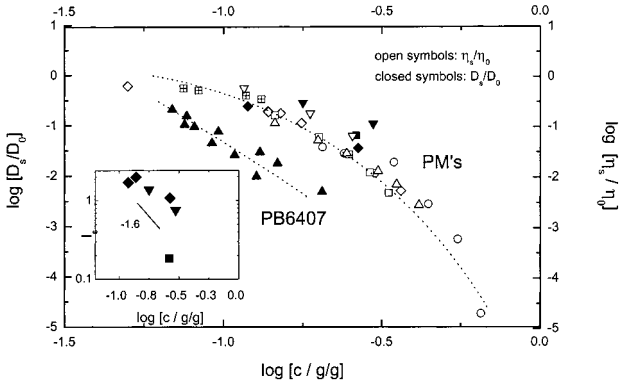

Figure 4. Concentration dependence of diffusion coefficient of the slow mode (attributed to self-diffusion, see text) D_s, normalized to the translational diffusion coefficient, D_0 (PMM40-g-S20, ■; PMM40-g-S20/PMM10-g-S20, ▼; PMM40-g-S20/PMM10-g-S110, ◆; PB6407, ▲). For comparison, the inverse normalized (η_s/η_0) solution viscosity is also shown (PMM40-g-S20, □; PMM10-g-S20, ⊞; PMM10-g-S110, △; PMS10-g-S100, ○; PMM40-g-S20/PMM10-g-S20, ▽; PMM40-g-S20/PMM10-g-S110, ◇). Dotted lines are drawn to guide the eye. Inset: respective concentration dependence of the intensity I_s. The solid line with slope −1.6 represents the scaling for I_s (eq 3).

judged from the multiarm stars behavior.[3] Furthermore, all PM samples exhibit a concentration scaling of the normalized intensities which is intermediate between the semidilute value $c^{-1.3}$ of flexible linear homopolymers and that of multiarm stars (eq 1). This becomes apparent through the comparison with the multiarm polybutadiene star PB6407, whose limiting I/cM value at small c was shifted to match the differences in the $(dn/dc)^2$ in Figure 2. The intermediate behavior of the osmotic modulus of the PM's further suggests a longer interpenetration of their arms compared to the case of multiarm stars; at a given $c/c^* > 1$, PM's have a lower $(\partial\Pi/\partial c)_{P,T}$, which is also reflected in the D_c/D_0 and D_p/D_0 ratios (Figures 3 and 4). On the other hand, the deviations of I/cM at $c < c^*$ from a master curve, which amount to a difference of about a factor of 2 (between PMM40-g-S20 and PMM10-g-S110), are beyond experimental error and unexpected (when compared to the respective behavior of multiarm stars).[4] One origin for the observed behavior could be the small differences in the refractive index contrast dn/dc to the solvent toluene mainly due to the presence of PS; PMMA is almost isorefractive with this solvent. However, this is not very likely to contribute much in view of the observed differences between PMM40-g-S20 and PMM10-g-S110. A partial contribution from a small uncertainty in the molecular weight determination is also conceivable.

Figure 3 depicts the cooperative diffusion D_c for the total concentration fluctuations with associated intensity I_c as a function of c, whereas its inset represents a master plot of the normalized diffusion coefficient D/D_0 vs c/c^* for the PM's of Figure 2. For dilute solutions ($c < c^*$), D_c becomes the translational diffusion coefficient D_0 (and I_c becomes I_0), which clearly depends on the total molecular mass (compare PMM40-g-S20 and PMM10-g-S20) and overall star shape (compare PMM40-g-S20 and PMM10-g-S110). For multiarm stars, the concentration dependence of D_c above c^* is theoretically derived accounting again for the core/shell contributions:[4]

$$\frac{D_c}{D_0} \approx c^{0.77}\left[1 - 0.21\delta\left(\frac{c}{c^*}\right)^{-1.3}\right] \qquad (2)$$

Equation 2 predicts a strong increase (the term containing δ) of D_c with concentration compared to the linear chain semidilute scaling[23] $c^{0.77}$. On the basis of the data of Figures 2 and 3 as well as eqs 1 and 2, it follows that the macromolecular (starlike or comblike) architecture effects (correction terms) are more pronounced for I_c than for D_c; the relative effect on these quantities is $(1 + \delta)/\delta$, a quantity which can be large for small δ. In fact, the behavior of PB6407 in Figure 3 virtually conforms to the semidilute scaling in sharp contrast to its cooperative intensity (Figure 2). Unexpectedly, for the present polymacromonomers D_c/D_0 approaches the semidilute prediction ($\sim c^{0.77}$) (inset, Figure 3) at $c > c^*$; on the other hand, the D_c data of the PM's can be superimposed in the D/D_0 vs c/c^* representation. Since $D_c = kT[\partial\mu/\partial c]_{T,P}/f_c$ with the f_c being the monomeric cooperative friction coefficient, a possible cause for the observed deviation might be the osmotic modulus of Figure 2. In fact, the obtained f_c is found to increase monotonically with concentration and superimpose when plotted against c/c^*.

In summary, the important finding concerning the relaxation of the total concentration fluctuations is that the semidilute properties of the PM's, namely the osmotic compressibility and the cooperative diffusion, clearly deviate from the corresponding properties of the high functionality multiarm star polymers[4] and the linear chains. On the basis of the theoretical description of the stars, the behavior in semidilute solution depends on the interaction free energy that reflects the monomer density inhomogeneity due to arm stretching.[4] Whereas the osmotic compressibility exhibits a concentration dependence intermediate between linear chains and hyperstars, the cooperative diffusion displays a weaker concentration dependence than the semidilute good solvent scaling; these are tentatively attributed to the stronger arm interpenetration in the case of decrease of PM's.

Self-Diffusion and Viscosity. As already mentioned above and demonstrated in ref 3, hyperstar self-diffusion is resolved in light scattering via functionality (size) polydispersity. For such spherical objects with functionality polydispersity ϵ, the star density fluctuations are obtained from the second-order expansion of the free energy in terms of fluctuations in ϵ, leading to an intensity[4]

$$I_s \sim \frac{f^2\epsilon^2}{N} c^{-1.6} \qquad (3)$$

The salient features of this derivation are the contribution of the osmotic free energy of semidilute linear chains, the ideal gas entropy of mixing of the stars, and the interaction energy due to chain stretching (inherent to star architecture) to the total free energy of the system. The very weak I_s in the present polymacromonomers with arm functionality $f = 10$ (PMM10-g-S110; essentially unresolved, Figures 1 and 2) and 40 (PMM40-g-S20; barely resolved, Figures 1 and 2) probably reflects very small polydispersity ϵ and low functionality f (eq 3). Actually, only for PMM40-g-S20 at a concentration of about 25% is there unambiguous evidence of a self-diffusion process; this assignment is also justified on the basis of the good agreement with the solution's zero-shear viscosity data of Figure 4.

To enhance I_s, we have increased the ϵ of PMM40-g-S20 via mixing[20] with either PMM10-g-S110 or PMM10-

g-S20 at a mass composition ratio 60:40 and different total polymer concentrations in toluene. The result is evident in Figure 1, which demonstrates the clear emergence of a second process in the relaxation function $C(q,t)$ and the distribution of relaxation times $L(\ln \tau)$ for the PMM40-g-S20/PMM10-g-S20 mixture in toluene. The intensity I_s and the diffusion coefficient D_s are plotted as a function of concentration in Figure 4. Since this process is essentially driven by the ideal entropy of mixing, the mixture's mutual diffusion coefficient essentially coincides with the effective self-diffusivity D^*_s, which is a function of the individual components self-diffusion coefficients. The inset of Figure 4 shows the concentration dependence of the extracted intensities I_s. The data are rather limited to extract safe conclusions, but a departure from the behavior of multiarm stars (eq 3) is apparent. Note that the decrease of intensity with increasing concentration, due to the interacting hairs, as per eq 3 and in analogy with the multiarm stars behavior, is well resolved.

On the basis of the above considerations, a favorable comparison of the measured D_s with the zero-shear viscosity of the solution (η_0) would further support this assignment, under the assumption of the validity of the Stokes−Einstein relation. Indeed, for the two mixtures PMM40-g-S20/PMM10-g-S110 and PMM40-g-S20/PMM10-g-S20 the normalized (known as relative) inverse zero-shear viscosity η_s/η_0 (where η_s is the solvent viscosity) exhibits virtually the same concentration dependence with the measured normalized diffusion D/D_0 as seen in Figure 4. This result is consistent with the respective behavior of the self-diffusion in multiarm stars[4b] and the long-time diffusion in hard sphere colloidal suspensions[24] and ultrasoft colloidal micelles.[25] For comparison, the corresponding data for the PB6407 multiarm star are also included in Figure 4. In the dilute limit $c \rightarrow 0$, both normalized diffusion and normalized viscosity tend toward 1, as expected. The zero shear viscosities of the polymacromonomers PMM10-g-S20, PMM40-g-S20, PMM10-g-S110, and PMS10-g-S100 were also measured and included in Figure 4. All viscosities exhibit the same concentration dependence within experimental error and are further comparable at the concentration range investigated. This similarity in behavior is not surprising, given the molecular structure and the similar total molecular masses of the materials.

The concentration dependence of the relative viscosity is depicted in a normalized plot in Figure 5, where c/c^* relates to the effective volume fraction (φ) of the PM's. In this figure the respective data from PB6407 in cyclohexane are also included for comparison.[26] This plot is useful in determining the effective softness of hairy suspensions through their departure from the hard sphere limit, which is depicted with the solid curve, following the Kreiger−Dougherty relation with a close packing volume fraction of $\varphi_p = 0.5$:[27]

$$\eta_r = \left(1 - \frac{\phi}{\phi_p}\right)^{-[\eta]\phi_p} \qquad (4)$$

where η_r is the relative (to the solvent) zero shear viscosity and the intrinsic viscosity $[\eta]$ assumes Einstein's value of 2.5 for hard spheres. The comparison with the regular hyperstars is based on the fact that these systems serve as models, and we seek to assess the deviations from these models, observed in the PM's;

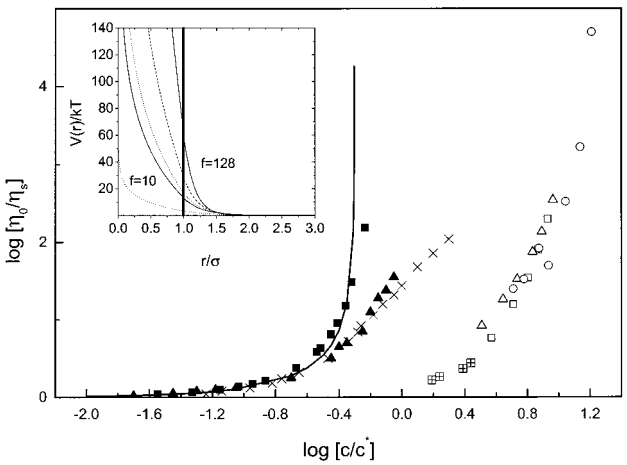

Figure 5. Master plot of the reduced viscosity η_0/η_s as a function of the effective volume fraction $\varphi = c/c^*$ for the PM's (same symbols as in Figure 4); in addition, data for multiarm star polymers with functionality $f = 128$ (■, $M_a = 80\,000$ g/mol), the $f = 6407$ (▲, $M_a = 7000$ g/mol), and $f = 32$ (×, $M_a = 80\,000$ g/mol) are also included for comparison. The solid curve represents the Krieger−Dougherty equation for hard spheres with a close packing volume fraction of $\varphi_p = 0.5$ (see text). Inset: effective interaction potential for star polymers[26] (normalized per kT, k being the Boltzmann constant) as a function of the normalized interstar distance (σ represents the star hydrodynamic radius) for different values of functionality, indicating the enhanced softness at low f values. From left to right, $f = 10$, 32, 40, 64, and 128. The solid vertical line represents the hard sphere repulsion.

the same justification holds for the use of eq 4 for comparison purposes, something that has been suggested in the literature as well.[28] In the present case, it is interesting that all PM data essentially collapse into a master plot (with a slight departure for the PMS10-S100 data) with an effective critical volume fraction $c/c^* \cong 16$ (although the data for each system are not sufficient to allow for accurate individual fits of eq 4), which is roughly 10 times larger than the respective volume fraction of PB6407. This is indeed a remarkable result, corroborated by the fact that a significant departure of the relative viscosity from unity occurs at $c/c^* \cong 2$ for the PM's and $c/c^* \cong 0.2$ for PB6407. This finding suggests that whereas in the stars even a weak interpenetration may have drastic impact on the dynamics, for the PM's a strong intepenetration is needed in order to obtain noticeable influence on the dynamic response. For the stars the resulting outward force scales as $f^{3/2}$.[29] The inset of Figure 5 depicts the ultrasoft interaction potential $V(r)/kT$ of star polymers[30] for different functionalities (normalized with the thermal energy kT). It is apparent that the enhanced softness of the repulsive forces as the functionality decreases is manifested in the deviation of the reduced viscosity from the hard sphere limit. This is demonstrated by comparing the results of PB stars with $f = 128$, 64, and 32 in this figure, which are in order in increasing softness. On the other hand, this will still not explain fully the sharp deviation of the PM's and the virtual collapse of viscosity data for $f = 10$ and $f = 40$ (given the fact that the potential under consideration is not derived of course for polymacromonomers). Therefore, the implication of the effects of the nonspherical shape (which yields much lower c^* compared to respective spherical objects) are clearly evident, whereas the analogy with the DLS data and in particular the difference of $C(q,t)$ between multiarm stars (two-step decay) and PM's

Table 2. WLF Constants for the Polymacromonomers Used Referred to Their Glass Transition Temperature

sample	T_g (K)[a]	C_1^g	C_2^g (K)
PMM10-g-S20	363	11.5	56
PMM40-g-S20	341	18.5	28
PMM10-g-S110	376	11.2	63
PMS10-g-S100	376	13	49
PMM40-g-S20/PMM10-g-S110	356	11.8	60
PMM40-g-S20/PMM10-g-S20	348	14.1	47

[a] Measured with differential scanning calorimetry (DSC), using a Rheometric Scientific PL-DSC instrument with heating rates of 10 and 20 K/min.

(single process, probably due to the small *f*) in the early semidilute regime is worth noting. Further, in analogy to the viscosity behavior, the concentration dependence of the self-diffusion coefficient of the PM's is different than that of multiarm stars; within the uncertainty of the limited data available, the difference of c/c^* between these two classes of materials for observing a departure of D_s/D_0 from the dilute limit behavior virtually matches that of the viscosity. Further, it is noted that the weak liquidlike structure (lower inset of Figure 1) and its reorganization do not affect significantly the solution's zero shear viscosity as confirmed by the examined validity of the Cox−Merz rule $\eta(\omega\rightarrow 0) \approx \eta(\dot{\gamma}\rightarrow 0)$.[31]

Behavior of Undiluted Systems. The dynamics in the melt was investigated with dynamic frequency sweeps in a wide temperature range from 90 to 170 °C. All samples investigated were found to be thermorheologically simple (with the same reference temperature T_r = 110 °C, above the glass transition temperature) as they obeyed the principle of time−temperature superposition with the (horizontal) shift factors α_T following the well-known WLF behavior,[32] $\log \alpha_T = -C_1(T - T_r)/(C_2 + T - T_r)$. The extracted WLF coefficients C_1 and C_2 are transformed[32] to C_1^g and C_2^g at the glass transition temperature T_g and presented in Table 2 along with the T_g's. The C_1^g and C_2^g values of the anisotropic PMM40-g-S20 clearly deviate from the other samples, apparently due to differences in macromolecular architecture. At this point the glass transition temperatures (T_g) of the bulk PM's measured by differential scanning calorimetry and reported in Table 2 should be discussed. It is evident that the T_g's of all PM's are lower than the respective T_g's of linear polystyrenes of comparable molecular masses; in particular, several nearly monodisperse (M_w/M_n < 1.1) linear PS from Polymer Source, Canada, were measured, with molecular weights ranging from 1500 to 120 000 g/mol, and their T_g's are depicted in Figure 6. The reduction in the T_g's of the PM's compared to the respective linear PS's is attributed to the excess free volume due to the free ends of the arms, and as such it is more dramatic for the higher functionality PMM40-g-S20. For the PM's having long branches, the T_g difference from the high molecular mass linear PS is smaller. These considerations are in agreement with earlier findings on a wide range of similar PM's.[11] Further, by using the plot of Figure 6, we can estimate the effective molecular weight of linear PS having the T_g of the PM studied (indicated by arrows). The fact that PMM40-g-S20, PMM10-g-S20, and PMM10-g-S110 or PMS10-g-S100 have T_g's of linear PS's with M_w = 2000, 6500, and 33 000 g/mol, respectively, shows the dramatic effect of chain end effects and implies easier processability of the PM's.

Further, as can be seen in the G' and G'' master curves of Figure 7, all samples exhibit Rouse-like

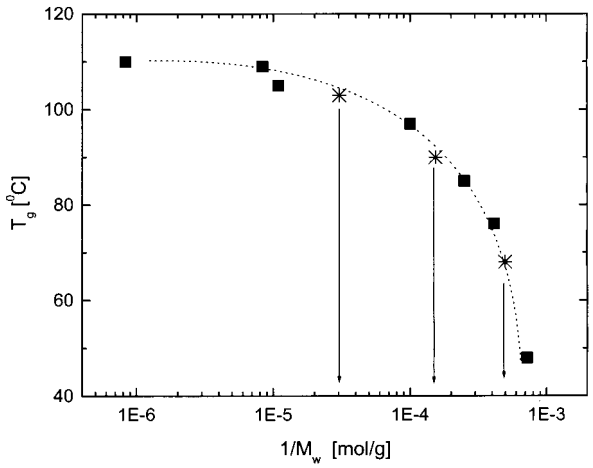

Figure 6. Dependence of the T_g of linear nearly monodisperse polystyrenes (■) on the inverse molecular mass. The dotted line is drawn to guide the eye. The polymacromonomers measured with T_g's of 68, 90, and 103 °C (see Table 2) are also shown (*); the arrows indicate the extracted effective linear PS molecular weight (see text).

behavior[32] with a clear well-defined flow region $G' \sim \omega^2$, $G'' \sim \omega$, a higher frequency transition region $G' \sim G'' \sim \omega^{1/2}$ without entanglement plateau, and a segmental relaxation detected at the highest frequencies. The absence of entanglement plateau is expected as both PS and PMMA branches have molecular masses (Table 1) below their entanglement molecular masses, M_e; the latter assume values 13 300 and 10 000 g/mol for PS and PMMA, respectively.[33,34] In fact, within the experimental uncertainties the PMM10-g-S110 has PS branches with molecular mass of about M_e, but this is not enough to form transient physical networks, as demonstrated in Figure 7. Moreover, the M_e of PM is clearly higher than that of the respective linear analogue of the backbone, because of the M_e's dependence on the molecular cross-sectional area.[11] Therefore, for the systems investigated, exhibiting total molecular mass above their M_e's, these features represent a clear proof that the grafted arm relaxation controls the dynamics of the polymacromonomers, in direct analogy to the behavior of multiarm stars and comb polymers. A further evidence of the starlike behavior of the PM's in the melt comes from the measurement of the linear viscoelastic spectrum of a linear unentangled PS with molecular mass about 10 000 (from Polymer Source, Inc., Canada), which is qualitatively identical to that of PMS10-g-S100. This indicates that the latter with a much higher total molecular mass exhibits the same relaxation behavior with the small linear chains; the only way to explain this is on the account of the arm relaxation as the mechanism controlling the dynamics of PMS10-g-S100. Therefore, all polymacromonomers studied exhibit behavior analogous to stars or comb polymers, where the dynamics is governed by the independent individual relaxation of the grafted chains,[4,35] in addition to the possible presence of slower modes of motion such as structural rearrangements or backbone-related processes;[35,36] as the arms are unentangled in the present PM's, their relaxation is of course Rouse-like (see also Figure 8).

A compilation of the dynamic results of various branched polymers is presented in Figure 8, which depicts the normalized arm relaxation time (to the segmental time) τ_R/τ_s as a function of the arm degree of

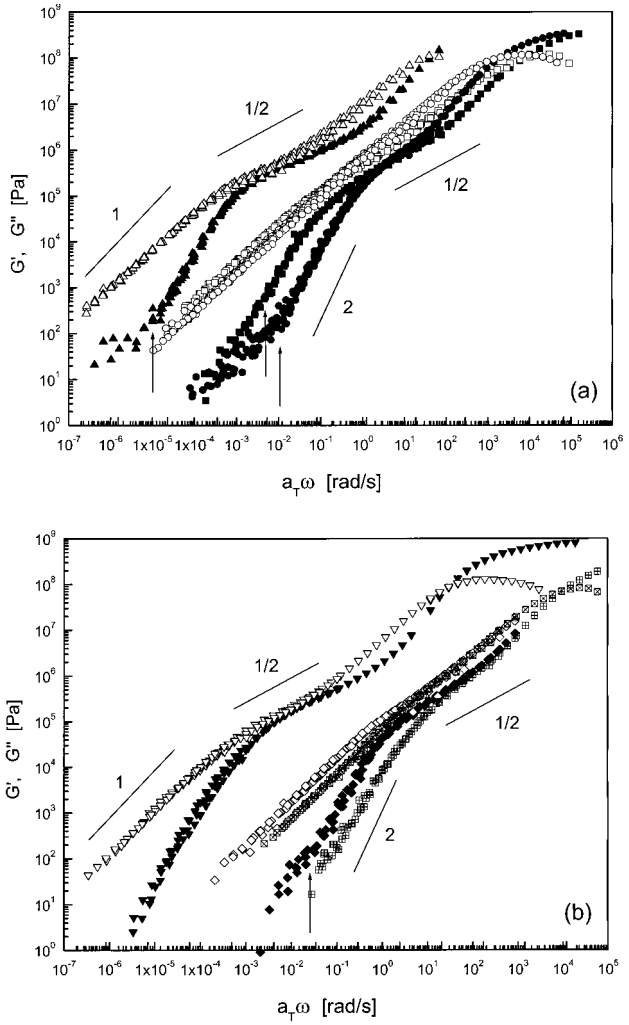

Figure 7. (a) Storage (G', closed symbols) and loss (G'', open symbols) master curves (covering the temperature range 90−170 °C) referred to T_r = 110 °C, for the four polymacromonomers investigated: PMM10-g-S20 (○), PMM40-g-S20 (□), PMM10-g-S110 (△). Lines with slopes 1, 2, and $^1/_2$ indicate terminal and intermediate flow regimes as discussed in the text. Vertical arrows indicate the onset of the slow modes (see text). (b) Respective data for PMS10-g-S100 (▽) and the two mixtures (PMM40-g-S20/PMM10-g-S20, crossed □; PMM40-g-S20/PMM10-g-S110, ◇).

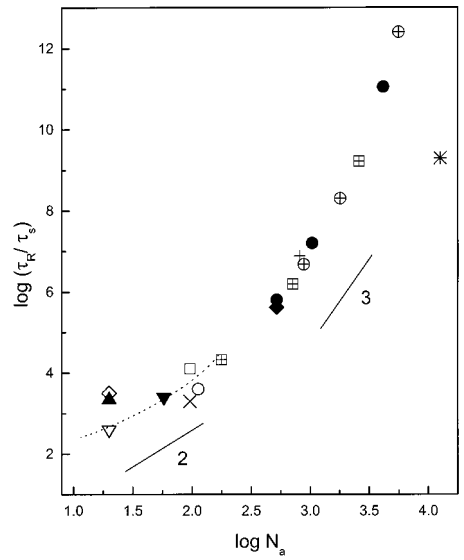

Figure 8. Normalized arm relaxation times τ_R (to the segmental times, τ_s) as a function of the degree of polymerization of the arm (N_a) for various branched polymers: regular and multiarm stars (polyisoprenes with f = 4 (⊗) and f = 18 (crossed □); polybutadienes with f = 4 (+), f = 64 (◆), and f = 128 (●);[5,35] polymacromonomers (PMM10-g-S20, ▽; PMM40-g-S20, ◇; PMM10-g-S110, ○; PMS10-g-S100, □), and blends (PMM40-g-S20/PMM10-g-S20, ▲; PMM40-g-S20/PMM10-g-S110, ▼). A linear unentangled polystyrene with M_w = 10 000 (×) and a linear entangled 1,4-polybutadiene with M_w = 165 000[5] (*) are also included for comparison. The dotted line represents simulation data for various stars, extracted from ref 34, whereas the lines with slopes 2 and 3 represent the typical unentangled Rouse and entangled scalings, respectively.

polymerization, N_a. This generalized master plot, which allows comparison under isofriction conditions, i.e., correcting for the difference in T_g's, includes arm relaxation data from different polyisoprene (f = 4, 18) and polybutadiene (f = 4, 64, 128) stars,[5] all with $N > N_e$, exhibiting stronger molecular mass dependence compared to linear chains, as already established.[5,36] The PM's of Table 1 and the two blends (discussed below) studied all lie in the untentangled regime, and in this respect these data extend the master curve of Figure 8 to the low N_a limit. It is interesting to note that all data are consistent and further in good agreement with respective simulation results of star systems,[37] indicated by the dotted line. An interesting finding is the distinct behavior of the clearly anisotropic PMM40-g-S20, suggesting the need to properly account (theoretically) for the shape effects on the dynamics.[14] The relaxation time of the linear unentangled PS (with M_w = 10 000) is also included with the remark that despite the fact that at low molecular masses the effects of architecture (stars vs linear chains)[37,38] on the dynamics are weak in comparison to the entanglement regime, the PMS10-g-S100 topology is still largely responsible for the observed difference in terminal dynamics, amounting to about 1 decade. Likewise, the well-entangled linear 1,4-polybutadiene (with M_w = 165 000 g/mol) is much faster than the respective stars of same molecular mass, as expected.[35−38]

A feature worth mentioning is the clear hint of a second terminal relaxation process at low frequencies,[39] which is unambiguously resolved in Figure 7 (its onset in the frequency domain being indicated by arrows). This is especially pronounced in samples PMM10-g-S20 and PMM10-g-S110, as well as the mixtures, and could relate to some cooperative rearrangements of the soft ordered polymacromonomers, in agreement with the SAXS results[40] and earlier analogous investigations on multiarm stars,[5,36] and as such it represents the signature of the soft order on the dynamics in the melt; alternatively, it could also relate to the relaxation of the backbone, in particular for the PMM40-g-S20 sample, whereas a small polydispersity contribution cannot be excluded, as already discussed above in the context of solutions.

The interest in studying blends of polymacromonomers stems primarily from the potential of such polymers to exhibit a rich phase behavior, from phase separation due to size difference to the formation of liquid crystalline mesophases,[11,20,41] depending on the arm size and functionality (thus anisotropy). In such cases the possible immiscibility between different PM's or PM and linear chain, all of the same chemistry, is due to topological reasons and in particular to an extra entropic contribution to the free energy of mixing, which

is related to the architecture-induced conformational asymmetry between components.[20,42] In addition, blending even in the miscible region might influence the dynamics through the enhancement of the polydispersity, as already seen in the case of solutions before. Two different blends were used in this work, namely PMM40-g-S20/PMM10-g-S110 (different arm molecular mass and functionality, similar total molecular mass) and PMM40-g-S20/PMM10-g-S20 (different functionality and total molecular mass, same arm molecular mass), both with 60% weight composition in PMM40-g-S20. Despite the weak enthalpic effect due to the PMMA backbone and PS branches, the main contribution to the free energy is expected to be the effect of chain architecture. In the present case, however, both blends were found to be miscible at all times (much like blends of multiarm star polymers considered in ref 20) in the temperature region investigated, as judged by the following: (i) The DSC measurements, revealing a single T_g in both cases; for PMM40-g-S20/PMM10-g-S110 $T_g = 83$ °C whereas for PMM40-g-S20/PMM10-g-S20 $T_g = 75$ °C. In both cases the glass transition temperature was below that of the respective linear polymers and assumed intermediate values between the two components (Table 1), following the Fox−Flory relation. (ii) Visual observations suggesting the presence of transparent phases at all temperatures. (iii) Linear viscoelastic measurements suggesting that both blends exhibit the same qualitative features as the single components. In particular, there is a single clear relaxation process attributed to arm relaxation, and weak slow process, barely resolved, should relate to structural relaxation as already discussed.

The interesting feature is that even for the blend PMM40-g-S20/PMM10-g-S110 there is one arm relaxation process despite the different size of arms of the two components (differing by a factor of 5); the arm length is known to control the arm relaxation process.[35] Furthermore, referring to Figure 8, a consideration of average molecular masses based on the composition of each blend suggests that the relaxation time data fit into the master plot for different stars and PM's (given the deviation of PMM40-g-S20 as discussed above); this implies that to a first approximation the dynamic properties of the blends of PM's can be understood by considering an average effective hairy starlike structure. For the mixture PMM40-g-S20/PMM10-g-S110 where both components exhibit virtually the same dynamics, the blend possesses nearly the same relaxation time. On the other hand, the blend PMM40-g-S20/PMM10-g-S20, which is characterized by a distinct difference in the components dynamics (more than 1 decade), essentially follows the slower component PMM40-g-S20, in qualitative agreement with the D_s behavior of this system in solution (Figure 4). Finally, these results suggest that blending of certain types of PM's (depending on arm number and size) at various compositions can be used as a means to effectively obtain intermediate molecular masses for studying the effects of molecular parameters on their properties. Such an approach has been successfully utilized in mixtures of symmetric diblock copolymers at certain range of molecular masses of the components.[43]

IV. Concluding Remarks

This study has demonstrated that polymacromonomers are very useful in expanding the general picture of dynamic response of branched polymers exhibiting both polymeric and colloidal features, as they are governed by the same basic physics (arm relaxation); on the other hand, consideration of the induced anisotropic shape is clearly needed in order to predict their dynamics accurately. The investigation of structure and dynamics in solution and in the melt yielded many common features with multiarm stars concerning their soft liquidlike ordering and their dynamic response, the latter controlled by arm relaxation and self-diffusion or structural rearrangements (in the melt). However, the concentration dependence of the transport properties of the present systems deviates from the scaling laws of stars, possibly because of their nonspherical shape and the larger interpenetration needed to observe the effect of ordering on the dynamic response. Blending such systems resulted in miscible mixtures at all times and allowed detecting the self-diffusion modes, identifying which component controls the overall relaxation process, and finally obtaining a wide range of effective intermediate molecular masses, depending on composition. Finally, it may be noted that the quantitative comparison of the properties of PM's with regular stars can be considered as preliminary, since hyperstars exactly comparable with the present PM's in terms of molecular dimension and functionality are not available yet.

Acknowledgment. It is a pleasure to acknowledge support of this research from a joint PLATON Grant 97-040. We are grateful to A. Larsen and I. Chira for assistance with the measurements and to A. Barne and R. Meim for the SEC measurements and fractionation.

References and Notes

(1) Halpering, A.; Tirrell, M.; Lodge, T. P. *Adv. Chem. Phys.* **1992**, *100*, 31.
(2) Grest, G. S.; Fetters, L. J.; Huang J. S.; Richter, D. *Adv. Chem. Phys.* **1996**, *94*, 65.
(3) Roovers, J.; Zhou, L.-L.; Toporowski, P. M.; van der Zwan, M.; Iatrou, H. *Macromolecules* **1993**, *26*, 4324.
(4) Seghrouchni, R.; Petekidis, G.; Vlassopoulos, D.; Fytas, G.; Semenov, A. N.; Roovers, J.; Fleischer, G. *Europhys. Lett.* **1998**, *42*, 271. Semenov, A. N.; Vlassopoulos, D.; Fytas, G.; Vlachos, G.; Fleischer, G.; Roovers, J. *Langmuir* **1999**, *15*, 358.
(5) Vlassopoulos, D.; Pakula, T.; Fytas, G.; Roovers, J.; Karatasos, K.; Hadjichristidis, N. *Europhys. Lett.* **1997**, *39*, 617. Pakula, T.; Vlassopoulos, D.; Fytas, G.; Roovers, J. *Macromolecules* **1998**, *31*, 8931.
(6) Plentz-Meneghetti, S.; Rein, D.; Lutz, P. J. In *Stars and Hyperbranched Polymers. Polymer Frontiers;* Mishra, M. K., Kobayashi, S., Eds.; Marcel Dekker: New York, 1999.
(7) Ederle, Y.; Isel, F.; Grutke, S.; Lutz, P. J. *Macromol. Symp.* **1998**, *132*, 197.
(8) Tsukahara, Y.; Mizuno, K.; Segawa, A.; Yamashita, Y. *Macromolecules* **1989**, *22*, 1546.
(9) Beers, K. L.; Gaynor, S. G.; Matyjaszewski, K.; Sheiko, S. S.; Möller, M. *Macromolecules* **1998**, *31*, 9416. Beers, K. L.; Gaynor, S. G.; Matyjaszewski, K.; Sheiko, S. S.; Möller, M. *Macromolecules* **1999**, *32*, 8331.
(10) Nemoto, N.; Nagai, M.; Koike, A.; Okada, S. *Macromolecules* **1995**, *28*, 3854. Terao, K.; Hokajo, T.; Nakamura, Y.; Norisuye, T. *Macromolecules* **1999**, *32*, 3690. Terao, K.; Nakamura, Y.; Norisuye, T. *Macromolecules* **1999**, *32*, 711. Tsukahara, Y.; Kohjiya, S.; Tsutsumi, K.; Okamoto, Y. *Macromolecules* **1994**, *27*, 1662. Ito, K.; Tomi, Y.; Kawaguchi, S. *Macromolecules* **1992**, *25*, 1534.
(11) Tsukahara, Y. *Macromol. Rep.* **1995**, *A32*, 821. Tsukahara, Y.; Tsutsumi, K.; Okamoto, Y. *Macromol. Rapid Commun.* **1992**, *13*, 409. Namba, S.; Tsukahara, Y.; Kaeriyama, K.; Okamoto, K.; Takahashi, M. *Polymer* **2000**, *41*, 5165.
(12) Tsukahara, Y.; Ohta, Y.; Senno, K. *Polymer* **1995**, *36*, 3413.
(13) Wintermantel, M.; Gerle, M.; Fisher, K.; Schmidt, M.; Wataoka, I.; Urakawa, H.; Kajiwara, K.; Tsukahara, Y. *Macromolecules* **1996**, *29*, 978. Gerle, M.; Fischer, K.; Roos, S.; Müller,

A. H. E.; Schmidt, M.; Sheiko, S. S.; Prokhorova, S.; Möller, M. *Macromolecules* **1999**, *32*, 2629.
(14) Saariaho, M.; Ikkala, O.; Szleifer, I.; Erukhimovich, I.; ten Brinke, G. *J. Chem. Phys.* **1997**, *107*, 3267. Saariaho, M.; Subbotin, A.; Ikkala, O.; tenBrinke, G. *Macromol. Rapid Commun.* **2000**, *21*, 110.
(15) Shiokawa, K.; Itoh, K.; Nemoto, N. *J. Chem. Phys.* **1999**, *111*, 8165. Fredrickson, G. H. *Macromolecules* **1993**, *26*, 2825.
(16) Gauger, A.; Pakula, T. *Macromolecules* **1995**, *28*, 190. Rouault, Y.; Borisov, O. V. *Macromolecules* **1996**, *29*, 2605.
(17) Provencher, S. W. *Comput. Phys. Commun.* **1982**, *27*, 229.
(18) Berne, B. J.; Pecora, R. *Dynamic Light Scattering*; Wiley: New York, 1976.
(19) Strobl, G. R. *Acta Crystallogr.* **1970**, *26*, 367.
(20) Vlassopoulos, D.; Fytas, G.; Roovers, J.; Pakula, T.; Fleischer, G. *Faraday Discuss.* **1999**, *112*, 225.
(21) Jucknischke, O. Ph.D. Thesis, Westfälischen Wilhelms−Universität Münster, 1995.
(22) Hamley, I. W.; Fairclough, J. P. A.; Ryan, A. J.; Ryu, C. Y.; Lodge, T. P.; Gleeson, A. J.; Pedersen, J. S. *Macromolecules* **1998**, *31*, 1188. Loppinet, B.; Sigel, R.; Larsen, A.; Fytas, G.; Vlassopoulos, D.; Liu, G. *Langmuir*, in press.
(23) DeGennes, P. G. *Scaling Concepts in Polymer Physics*; Cornell University Press: New York, 1979.
(24) Segre, P. N.; Meeker, S. P.; Pusey, P. N.; Poon, W. C. K. *Phys. Rev. Lett.* **1995**, *75*, 958.
(25) Sigel, R.; Pispas, S.; Vlassopoulos, D.; Hadjichristidis, N.; Fytas, G. *Phys. Rev. Lett.* **1999**, *83*, 4666.
(26) Roovers, J. *Macromolecules* **1994**, *27*, 5359.
(27) Krieger, I. M.; Dougherty, T. J. *Trans. Soc. Rheol.* **1959**, *3*, 137.
(28) Solomon, M. J.; Boger, D. V. *J. Rheol.* **1998**, *42*, 929.
(29) Halperin, A.; Alexander, S. *Europhys. Lett.* **1988**, *6*, 329. Raphael, E.; Pincus, P.; Fredrickson, G. H. *Macromolecules* **1993**, *26*, 1996.
(30) Likos, C. N.; Loewen, H.; Watzlawek, M.; Abbas, B.; Jucknischke, O.; Allgaier, J.; Richter, D. *Phys. Rev. Lett.* **1998**, *80*, 4450.
(31) Macosko, C. W. *Rheology. Principles, Measurements and Applications*; VCH: New York, 1994.
(32) Ferry, J. D. *Viscoelastic Properties of Polymers*, 3rd ed.; Wiley: New York, 1980.
(33) Yurasova, T. A.; McLeish, T. C. B.; Semenov, A. N. *Macromolecules* **1994**, *27*, 7205. Roovers, J.; Graessley, W. W. *Macromolecules* **1981**, *14*, 766.
(34) Fetters, L. J.; Lohse, D. J.; Richter, D.; Witten, T. A.; Zirkel, A. *Macromolecules* **1994**, *27*, 4639.
(35) McLeish, T. C. B.; Milner, S. T. *Adv. Polym. Sci.* **1999**, *143*, 195.
(36) Kapnistos, M.; Semenov, A. N.; Vlassopoulos, D.; Roovers, J. *J. Chem. Phys.* **1999,** *111*, 1753.
(37) Pakula, T. *Comput. Theor. Polym. Sci.* **1998**, *8*, 21.
(38) Pakula, T.; Geyler, S.; Edling, T.; Boese, D. *Rheol. Acta* **1996**, *35*, 631.
(39) This situation should not be confused with slow modes encountered in rheometry or light scattering and typically attributed to polydispersity effects.
(40) It is noted that the SAXS data refer to solutions, but this soft order should persist in the melt as well, in analogy to the multiarm star behavior.[4]
(41) Tsukahara, Y.; Inoue, J.; Ohta, Y.; Kohjiya, S. *Polymer* **1994**, *35*, 5785.
(42) Fredrickson, G. H.; Liu, A. J.; Bates, F. S. *Macromolecules* **1994**, *27*, 2503.
(43) Floudas, G.; Vlassopoulos, D.; Pitsikalis, M.; Hadjichristidis, N.; Stamm, M. *J. Chem. Phys.* **1996**, *104*, 2083.

MA000634Q